EXPERIMENTS OF RISER SLUG FLOW USING TOPSIDE MEASUREMENTS: PART II

Heidi Sivertsen * **Vidar Alstad** ** **Sigurd Skogestad** *,[1]

* *Department of Chemical Engineering, Norwegian University of Science and Technology, Trondheim, Norway*
** *StatoilHydro Research Centre, Porsgrunn*

Keywords: Cascade control, unstable, poles, feedback control, controllability analysis

Previous experiments performed on a small-scale lab rig build at the Department of Chemical Engineering, NTNU showed that, despite noisy measurements, it is possible to stabilize the flow in the slug flow region using only topside measurements. The question to be answered in this paper is; do these results also apply for larger riser-systems?

In this paper we look at some results obtained from a 10m high, 7.6 cm diameter *medium* scale test rig located at Hydro's Research Park in Porsgrunn, Norway. Several cascade control structures are tested and compared; both with each other and the results obtained from the small-scale NTNU loop. Also in this case the rig was modelled and analysed using Storkaas' simple three-state model. The new experiments confirmed the results achieved using the small-scale rig. This suggests that the small-scale lab loop can be used as a tool to predict possible useful control strategies for the riser slug problem.

1. INTRODUCTION

The medium-scale multiphase flow control rig at Hydro's O&E research centre, located in Porsgrunn, is built to simulate multiphase flow in an offshore well/pipeline and production unit. The facility is ideal for development and testing of new control solutions for anti-slug and separator control under realistic conditions. Figure 1 shows a photograph of the facility.

Several experiments were performed to test similar control configurations as was also tested on the NTNU small-scale lab rig, described in Sivertsen and Skogestad (2008). This was done in order to investigate whether different scales have an effect on the quality of the control structures. Having results from a larger rig could give an indication on whether the small-scale NTNU lab rig really was suitable as a tool for finding good control solutions to be used in larger scale facilities, such as a production platform. The question was; could active control be used to stabilize the flow also for the medium-scale lab rig? In particular it was interesting to see whether or not only topside measurements could be used to stabilize the flow, as was done on the small scale lab rig described in Sivertsen and Skogestad (2008).

Fig. 1. A birds-view perspective of the medium-scale riser rig at Hydro's O&E research centre in Porsgrunn

2. EXPERIMENTAL SETUP

During the experiments the flow consisted of water and air. The pipe diameter is 7.6 cm (3") and the height

[1] Author to whom correspondence should be adressed: skoge@chemeng.ntnu.no

of the riser 10.0 m. The water inlet rate during the experiments was about 7-8 m^3/h . The air flow rate fluctuated between approximately 8 to 11 m^3/h. Slugging occurred for valve openings larger than about 12%. Figure 2 show a schematic overview of the layout and available instrumentation.

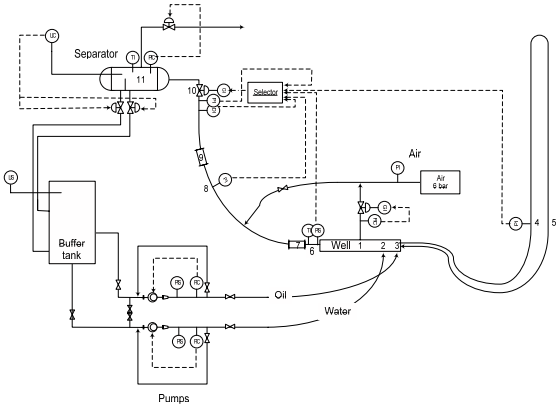

Fig. 2. Schematic overview of the layout and available instrumentation

2.1 Geometry

The loop includes an approximately 4 m long ”well section” where gas, oil and water are introduced through different inlets. This ”well section” consists of annulus and tubing, a 15.2 cm outer pipe and a 7.6 cm inner tubing with perforations. Since the tubing is perforated, the phases are assumed to have negligible momentum when entering the tubing. The pipe section consist partly of flexible tubing, hence it is possibly to vary the geometry of the piping. This way the inclination of the riser and other parts of the pipe can be adjusted to achieve the desired geometry.

The pipeline geometry during the experiments was chosen to give terrain-induced slugging. A more detailed schematic of the geometry used in the experiments is shown in Figure 3. The numbers indicate the location of feeding inlets and important instrumentation.

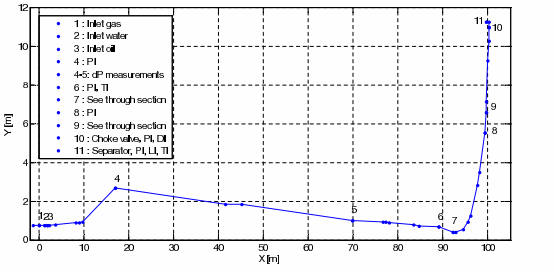

Fig. 3. Schematic of the geometry of the riser-system

The numbers 1, 2 and 3 indicate the air, water and oil inlets respectively. Downstream this section the pipeline is close to horizontal for about 10 m. An approximately 7 m, 35° inclined section then follows with a pressure measurement, P_1, at the end (4). The next 60 m section has a 1.8° declination, followed by an approximately 20 m horizontal section with a pressure and temperature measurement at the end (6). A low point in the geometry (7) is then followed by a 10 m long vertical riser. The low-point contains a see-trough section which makes it possible to visually determine the flow regime in this section. At the top of the riser a production choke (10) and separator (11) are located. There is also a pressure measurement (8) and a see-through section (9) located half-way up the riser. Just upstream the production choke a pressure measurement, P_2, and a gamma densiometer are implemented.

The water and oil outlets from the separator are returned to a large 10 m^3 buffer tank. The oil and water feed are pumped from this buffer tank back to the respective phase inlets in the well section using two displacement pumps. Before entering the well section, the feed flow rate of each phase is measured.

2.2 Gas feed

The compressed air is supplied from the local air supply net. The pressure is approximately 7 bara. An automated control valve controls the feed flow rate of compressed air to the well section. The operating range of the control valve is 10-400 kg/h. During experiments the feed flow of air is normally in the range 15 to 50 kg/h.

The mass flow and the density of the compressed air are measured using a Coriolis type mass flow meter.

2.3 Water feed

The feed flow rate of water is controlled by a replacement pump. The power is either set directly by the operator or given as output from a feedback controller using the volumetric flow rate as measurement.

The pumps are designed for flow rates up to 7 m^3/h with a pressure increase of 6 bar. Normal flow rates during experiments are 0-10 m^3/h.

Downstream the pumps, the pressure and the single phase flow rates are measured. The air flow rate is measured using a differential pressure volumetric flow meter (Pivot tube), while the water flow rate is measured using a Coriolis type mass flow meter with a maximum flow rate of 25 m^3/h.

2.4 Separator

The three-phase separator located at the top of the riser has a volume of approximately 1.5 m^3. A 53 cm high weir plate separates the oil and water outlets. The separator is equipped with a pressure measurement and measurements of the oil and water levels. During

the experiments presented here, no oil was added to the flow.

2.5 Control choke valve

The control choke valve is a vertically positioned valve located at the top of the riser. The valve is equipped with a Profibus-PA Positioner which returns the actual valve position to the control system.

2.5.1. Choke valve characteristics Several flow experiments have earlier been performed in order to find the single- and two-phase (water/air) valve characteristics. It is assumed that the following model describes the flow through the valve

$$Q = \overbrace{C_v f(z)}^{K(z)} \sqrt{\frac{\Delta P}{\rho}} \tag{1}$$

In this equation C_v is the valve constant and $f(z)$ is the characteristics of the valve. ΔP is the pressure drop across the valve and ρ is the density of the fluid. For valve openings less than 50% for single-phase and 60% for two-phase flow the characteristics were found to be close to linear. Equation (1) can thus be written

$$Q/C_v = z\sqrt{\frac{\Delta P}{\rho}} \tag{2}$$

Values for Q/C_v can be calculated from given values for valve opening z, measured pressure drop across the valve ΔP and measured density ρ.

2.6 Instrumentation

The rig is controlled from a control room located close to the rig. In addition to the temperature sensors, pressure sensors and gamma densiometer indicated in Figure 3, the instrumentation consists of single phase flow meters for the gas, oil and water inlet rates, oil and water level measurements of the separator and separator pressure and temperature measurements.

A number of automatic control valves are installed. This includes the production choke valve, the valves controlling gas, water and oil outlet from the separator and the feed flow of air to the well section. These valves can be operated either in manual mode or in automatic mode where valve openings are given as output from PID feedback controllers.

3. CONTROLLABILITY ANALYSIS

3.1 Modelling

In Sivertsen and Skogestad (2008) it was shown how an analysis of a model describing a *small*-scale lab-rig did reveal fundamental control limitations depending on which measurement that was used in the control configuration. This was found using a simplified model (Storkaas et al. (2003)). One of the advantages of this simple model is that it is well suited for controller design and analysis. It consists of three states; the holdup of gas in the feed section (m_{G1}), the holdup of gas in the riser (m_{G2}), and the holdup of liquid (m_L). The model is illustrated in Figure 4.

The same model was used to predict the behaviour for the medium-scale lab rig used in this study. Using this model the system was analysed in the same way as in Sivertsen and Skogestad (2008). Both open- and closed loop simulations have been performed.

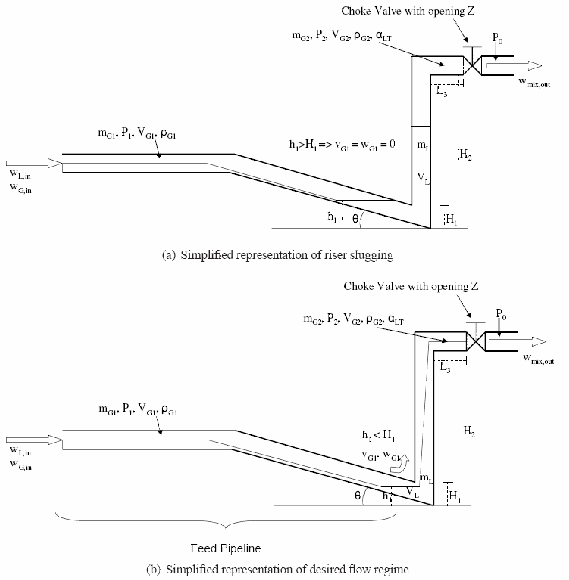

Fig. 4. Storkaas' pipeline-riser slug model (Storkaas et al. (2003))

After entering the geometrical and flow data for the lab rig, the model was tuned as described in Storkaas et al. (2003) to fit the open loop behaviour of the lab rig. The model data and tuning parameters are presented in Table 1. After inserting new system parameters and re-tuning the model, the open-loop data found using the model fitted the experimental results quite well as shown by the bifurcation plot in Figure 5.

The bifurcation diagram gives information about the valve opening for which the flow becomes unstable and also shows the amplitude of the pressure oscillations for the inlet and topside pressures (P_1 and P_2). The upper lines in the bifurcation plot show the maximum pressure at a particular valve opening and the lower line shows the minimum pressure. The lines meet at the "bifurcation point" when the valve opening is approximately 12%. This is the point where transition to slug flow occurs naturally and this is the highest valve opening which gives "non-slug" behaviour in open-loop operation; without control. The dotted line in the middle shows the unstable "non-slug" solution

Table 1. Model data parameters

Parameter	Symbol	Value
Inlet flow rate gas $[kg/s]$	$w_{G,in}$	0.0075
Inlet flow rate water $[kg/s]$	$w_{L,in}$	1.644
Valve opening at bifurction point [-]	z	0.12
Inlet pressure at bifurcation point $[barg]$	$P_{1,stasj}$	0.9
Topside pressure at bifurcation point $[barg]$	$P_{2,stasj}$	0.3
Separator pressure $[barg]$	P_0	0
Liquid level upstream low point at bifurcation point $[m]$	$h_{1,stasj}$	0.05
Upstream gas volume $[m^3]$	V_{G1}	0.2654
Feed pipe inclination $[rad]$	θ	0.05
Riser height $[m]$	H_2	10
Length of horizontal top section $[m]$	L_3	0.1
Pipe radius $[m]$	r	0.0381
Exponent in friction expression [-]	n	2.15
Choke valve constant $[m^{-2}]$	K_1	0.0042
Internal gas flow constant [-]	K_2	1.83
Friction parameter $[s^2/m^2]$	K_3	72.37

predicted by the model. This is the desired operating line with closed-loop operation.

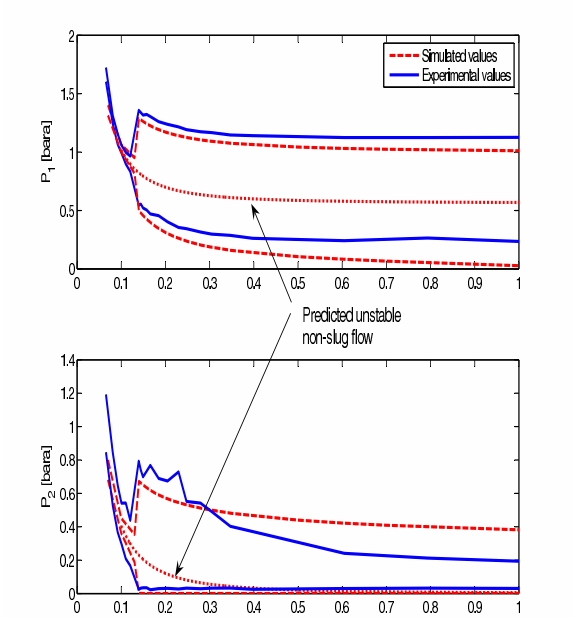

Fig. 5. Bifurcation plot for the medium scale rig: Pressures at inlet P_1 and topside P_2 as function of choke valve opening z

The bifurcation plot was obtained by open-loop simulations of the system at different valve openings. Some of these results are plotted in Figure 6 together with experimental results. The model fit the experimental data quite well, both in terms of amplitude and frequency of the oscillations. Note that a shift in time does not matter. The match between simulated and experimental results is especially very good for a valve opening of 14.5%.

In Figure 7 a root-locus diagram of the system is plotted. This shows how the poles, computed eigenvalues from the model, cross into the RHP as the valve opening reaches 12% from below. This confirms what was seen in the bifurcation diagram.

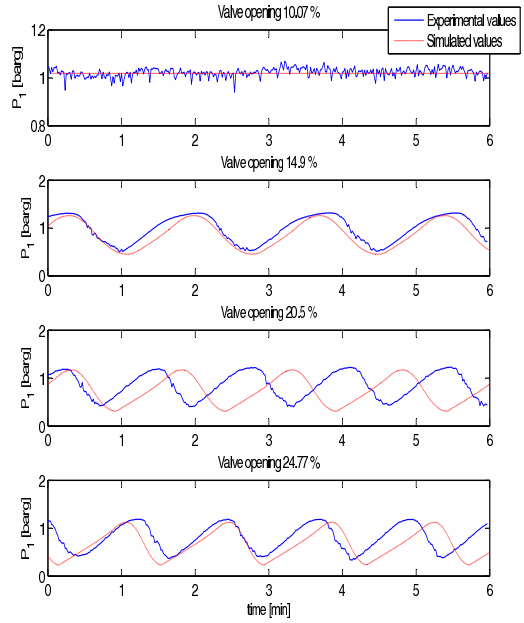

Fig. 6. Open loop data for valve openings 10, 15, 20 and 25%.

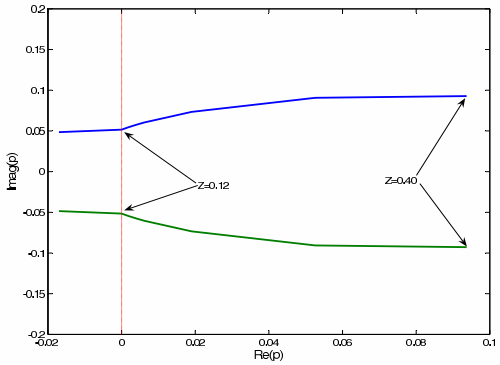

Fig. 7. Root-locus plot showing the trajectories of the RHP open-loop poles when the valve opening varies from 0 (closed) to 0.4

3.2 Analysis

The model can now be used to explore different measurement alternatives for controlling the flow. The following measurements were analysed in this study; inlet pressure P_1, pressure upstream production choke P_2, density ρ, mass flow rate F_W and volumetric flow rate F_Q through the topside choke. Figure 8 shows the different measurement candidates.

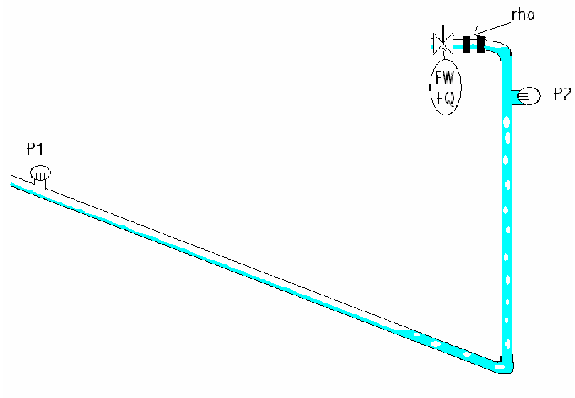

Fig. 8. Measurement candidates for control

In Sivertsen and Skogestad (2008) it was shown how the RHP poles and zeros and their locations compared to each other in the imaginary plane had a large influence on the controllability of the system. By scaling the system and calculating the sensitivity peaks it is possible to get a picture of the challenges in terms of stabilizing the system.

The process model G and disturbance model G_d were found by linearizing Storkaas' model at two operation points (z = 0.15 and z = 0.2). The models were then scaled as described in Skogestad and Postlethwaite (1996). The process variables were scaled with respect to the largest allowed control error and the disturbances were scaled with the largest variations in the inlet flow rates in the lab. The disturbances were assumed to be frequency independent. The input was scaled with the maximum allowed positive deviation in valve opening since the process gain is smaller for large valve openings. For measurements y=[P_1 P_2 ρ W Q] the scaling matrix is De=diag[0.1bar 0.1bar 50kg/m^3 0.2kg/s 1*10^{-3}m^3/s]. The scaling matrix for the disturbances d=[m_G and m_L] is Dd= diag [2*10^{-3}kg/s 0.2kg/s]. The nominal values are 0.0075 kg/s for the gas and 1.64 kg/s for the water rate. The input is scaled $Du = 1 - z_{nom}$ where z_{nom} is the nominal valve opening.

Tables 2 and 3 summarizes the results of the analysis. The location of the RHP poles and zeros are presented for valve openings 15 and 20%, as well as stationary gain and lower bounds on the closed-loop transfer functions described Sivertsen and Skogestad (2008). The pole location is independent of the input and output (measurement), but the zeros may move. From the bifurcation plot in Figure 5 it is seen that both of these valve openings are inside the unstable area. This can also be seen from the RHP location of the poles.

The only two measurements of the ones considered in this paper which introduces RHP-zeros into the system, are the topside density ρ and pressure P_2. The RHP zeros are in both cases located quite close to the RHP poles, which results in the high peaks especially for sensitivity function SG but also for S. In Figure 9 the RHP poles and relevant RHP zeros are plotted together. This plot shows that we can expect problems when trying to stabilize the flow using these measurements as single measurements.

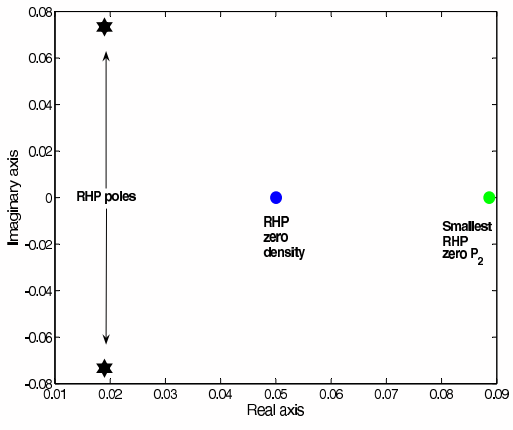

Fig. 9. Plot-zero map for valve opening 20%

The model is based on constant inlet flow rates. The stationary gain for F_W predicted by the model is 0, which means that it is not possible to control the steady-state behaviour of the system and the system will drift. Usually the inlet rates are pressure dependent, and the zeros for measurements F_Q and F_W would be expected to be located further away from the origin than indicated by Tables 2 and 3.

Figure 10 and 11 shows the Bode plots for the different plant models and disturbance models respectively. The models were found from a linearization of the model around valve opening 15%. Like in Sivertsen and Skogestad (2008) the Bode plots show that for the mass flow rate measurement F_W the value of the disturbance model $|G_dW|$ for low frequencies is higher than plant model $|GW|$. For acceptable control we require $|G(jw)| > |G_d(jw)| - 1$ for frequencies where $|G_d| > 1$ (Skogestad and Postlethwaite (1996)). In this case $|G_d(0)|$ is 1.01 and G_W is close to zero, which means problems can occur for this measurement.

3.3 Simulations

Closed-loop simulations were performed in order to investigate the effect of the limitations found in the analysis. The measurements were used as single measurements in a feedback loop with a PI-controller.

Table 2. Control limitation data for valve opening 15%. Unstable poles at $p = 0.0062 \pm 0.060i$.

Measurement	RHP zeros	Stationary gain	Minimum bounds				
		$\|G(0)\|$	$\|S\|$	$\|SG\|$	$\|KS\|$	$\|SG_d\|$	$\|KSG_d\|$
$P_1[bar]$	-	22.9	1.00	0.00	0.016	0.00	0.042
$P_2[bar]$	1.00, 0.09	20.5	1.21	15.6	0.017	0.54	0.040
$\rho[kg/m^3]$	0.051	33.1	1.22	33.4	0.011	1.02	0.042
$F_W[kg/s]$	-	0.00	1.00	0.00	0.006	0.00	0.042
$F_Q[m^3/s]$	-	8.3	1.00	0.00	0.013	1.02	0.040

Table 3. Control limitation data for valve opening 20%. Unstable poles at $p = 0.019 \pm 0.073i$

Measurement	RHP zeros	Stationary gain	Minimum bounds				
		$\|G(0)\|$	$\|S\|$	$\|SG\|$	$\|KS\|$	$\|SG_d\|$	$\|KSG_d\|$
$P_1[bar]$	-	10.1	1.00	0.00	0.082	0.00	0.090
$P_2[bar]$	1.08, 0.089	8.94	1.66	10.7	0.10	0.55	0.070
$\rho[kg/m^3]$	0.050	2.87	1.60	19.6	0.048	1.27	0.080
$F_W[kg/s]$	-	0.00	1.00	0.00	0.021	0.00	0.070
$F_Q[m^3/s]$	-	4.16	1.00	0.00	0.047	0.00	0.070

Figure 12 shows this control structure using the inlet pressure P_1 as measurement.

Figure 13 compares the simulation results obtained using four different measurement candidates. Disturbances in inlet flow rates for the gas and water are this time not included in the simulations. The results can for this reason differ somewhat from the results obtained in Sivertsen and Skogestad (2008). Despite this, the results were quite similar. Results using the topside pressure P_2 are not included in the plot, as the corresponding controller was not able to stabilize the flow.

At first, the controllers are turned off and the system is left open loop with a valve opening of 20% for approximately three and a half minute. From the bifurcation diagram in Figure 5 it was shown that the system goes unstable for valve openings larger than 12%. As expected the system oscillates due to the presence of slug flow.

When the controllers are activated the control valves start working as seen from the right plot in Figure 13. After about 80 minutes the setpoints are changed for all the controllers, bringing the flow further into the unstable region. The aim of the simulation study is to be able to control the flow with satisfactory performance as far into the unstable region as possible, which means with as high average valve opening as possible. Several simulations were performed, and the ones stabilizing the flow at the highest valve opening are presented in 13.

Like in Section Sivertsen and Skogestad (2008), the controllers giving the best results were the ones using inlet pressure P_1 and volumetric flow rate F_Q as measurements. However, this time the flow controller F_Q outperformed the pressure controller, being able to stabilize the controller with an average valve opening of impressing 55%. Based on earlier knowledge of slug control and experimental results; these results are to good to be true, and comes from the fact that no disturbances in the inlet flow rates were added in the simulations this time.

The results using the density and mass flow controller were quite similar to those obtained for the small scale lab rig in Sivertsen and Skogestad (2008). It was possible to control the flow in the unstable region, but the controllers were slow and did not manage to stabilize the flow very far into the unstable region. The analysis in Section 3.2 indicate that these problems stems from the RHP zeros introduced when using these measurements.

4. EXPERIMENTAL RESULTS

The analysis in Section 3.2 showed that both the inlet pressure P_1 and the scaled topside volumetric flow rate F_Q were suitable for stabilizing the desired non-slug flow pattern. The results using the topside density ρ were not as good as for P_1 and F_Q, but still it was possible to control the flow using also this measurement.

Figure 14 shows experimental results from an attempt to stabilize the flow using ρ as single measurement. Even though the controller stabilizes the flow initially, the flow eventually returns to the slug flow pattern. The fact that the flow is so quickly stabilized suggest that the density is better suited for control than the model predicts, in fact it stabilizes the flow at approximately 20% which is far better than the results found in the analysis. However, the controller seems to eventually drift from the desired setpoint causing the flow to become unstable.

Looking at Table 3 it is clear that except for the mass flow measurement F_W with zero steady-state gain, ρ is the measurement having the lowest steady-state gain at valve opening 20%. This explains why the controller does not seem to be able to keep the flow stable at the setpoint after the flow has been stabilized. Also for the volumetric flow rate measurement F_Q the steady-state gain is quite low for valve opening 20%,

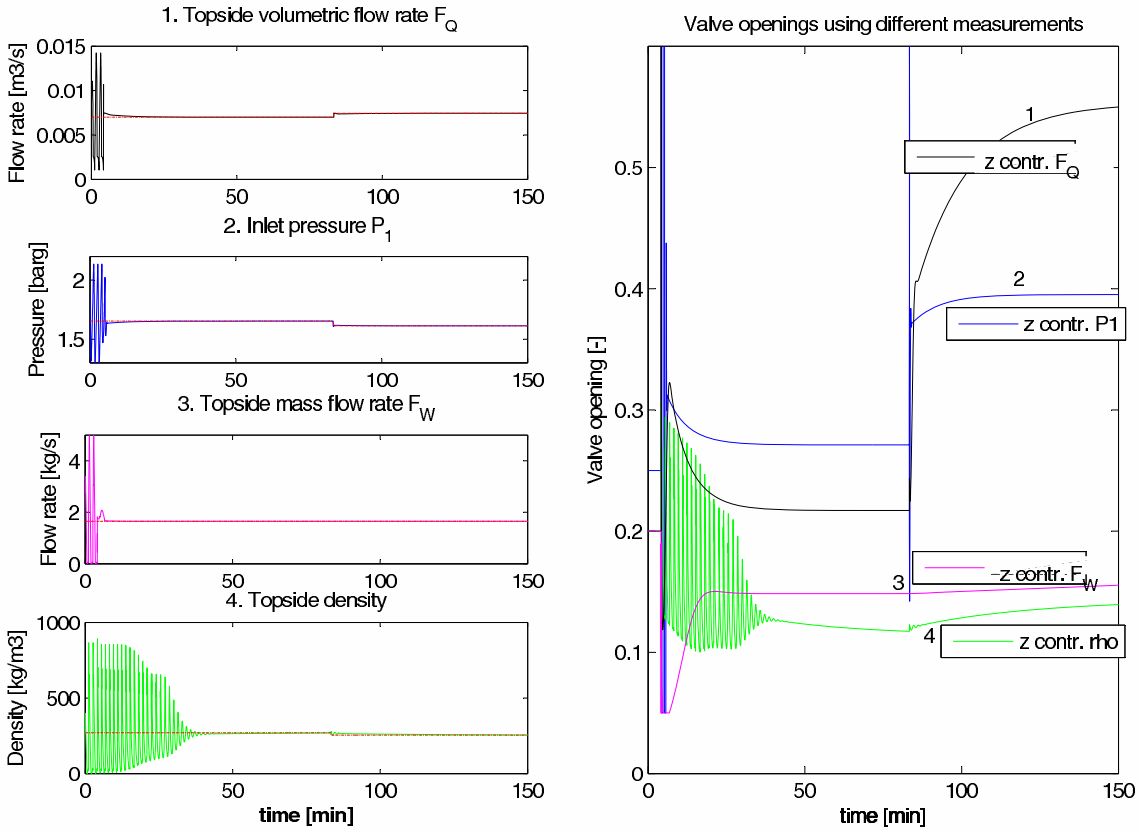

Fig. 13. Stabilizing slug flow using the choke valve (z); PI control with four alternative measurements

and we might expect the same problems using this measurement as the single measurement.

Control configurations using combinations of measurements can improve the performance of a controller when compared to controllers using single measurements. In order to avoid the drift problem, different cascade controllers were tested experimentally. Six cascade controllers were tested, using different measurement combinations. The measurements were combined in a cascade control configuration, where the setpoint for the inner controller is adjusted by the outer loop to prevent the inner controller from drifting. This way ρ and F_Q can be used as measurement in an inner loop, even though the controller based solely on one of these measurements suffer from the drift problem. The volumetric flow measurement used during the experiments was scaled with respect to the choke valve constant C_v.

Topside measurements are often noisy, and so also in this case. For this reason the density measurement signal was filtered using a first-order lowpass filter with a time constant of $4s$.

The inlet pressure P_1 was also used as measurements for the inner loop. Although P_1 is not a topside measurement and often not available in many real subsea applications, it was included to serve as a comparison for the other controllers. As outer measurements, the the pressure drop across the control valve P_2 and topside choke valve opening z were used. This gives all together six combinations of measurements in the outer and inner loop; (a) z and P_1 (b) z and ρ (c) z and F_Q (d) P_2 and P_1 (e) P_2 and ρ (f) P_2 and F_Q. Figure 15 shows a sketch of a cascade control structure for alterative (e) and Figures 16-18 shows the experimental results for all six alternatives.

All measurements have been filtered using a non-causal spline interpolation method to obtain a smooth estimate of the measurement. In the upper three plots the valve opening z is used as outer loop measurement. In the three lower plots the measured topside pressure P_2 is used.

During the experiments, the operation is gradually moved further into the unstable region by changing the setpoint in the outer loop (increasing z_S and decreasing $P_{2,S}$).The valve opening for which the flow can no longer be stabilized gives a measure on the performance of each controller. Note that being able to increase the mean valve opening and at the same time keep the flow stable has large economic advantages. This is because producing at a higher valve opening implies less friction loss and increased production.

The results using all of the controllers were very good, and they all managed to stabilize the flow far into the unstable region. The upper plot in each of the subfigures shows how the valve opening is increased during the experiments.

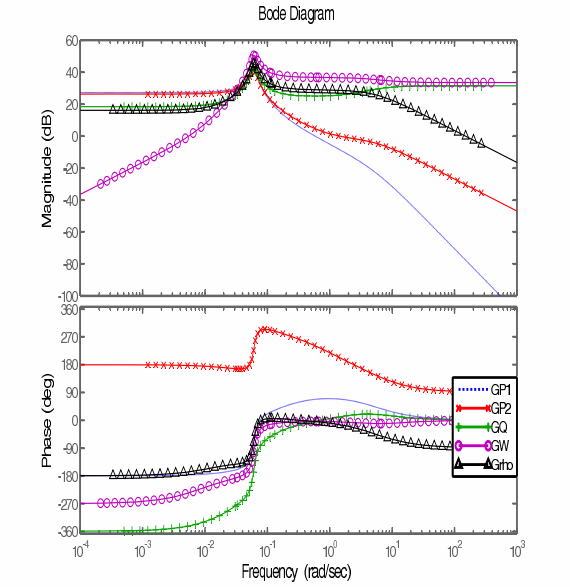

Fig. 10. Bode plots for the plant models using different measurements

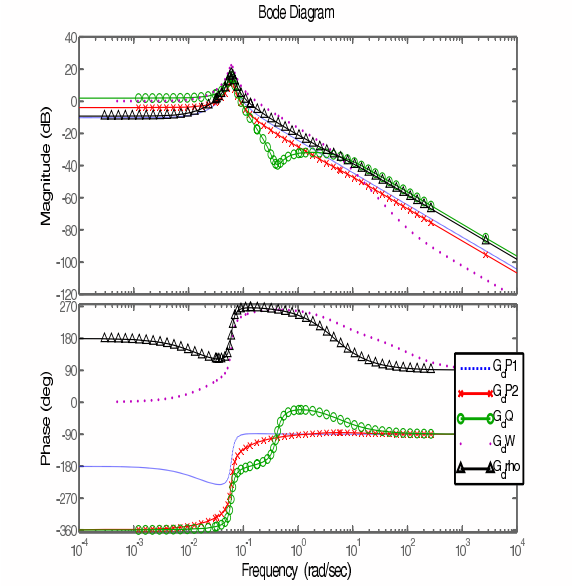

Fig. 11. Bode plots for the disturbance models using different measurements

Table 4 compare the average values the last 12 min before the controllers go unstable. As mentioned, the mean valve opening gives a good indication of the quality of the controller. See also Figure 19 in the Appendix which shows more detailed plots for all the controllers the last 12 minutes before instability.

Based on this, wee conclude that using P_2 in the outer loop and either P_1 or F_Q in the inner loop is the best choice with average maximum valve opening 23.8% and 23.9%, respectively. The third best choice is using z in the outer loop and F_Q in the inner loop (22.8%).

The controllers were not fine-tuned and the results might for this reason be influenced somewhat by the quality of the tuning. Still, the results showed that it was possible to stabilize the flow very well using only topside measurements and that these results are comparable to the results found when including subsea measurement P_1 as one of the measurements.

5. DISCUSSION

It is important to note that Storkaas' model used to analyse the system is a very simplified model, and it was used merely as a tool to see which problems might occur in the lab, and the underlying reasons for the problems. When comparing the experimental results with analysis and simulations using Storkaas' model prior to the experiments, it was clear that the

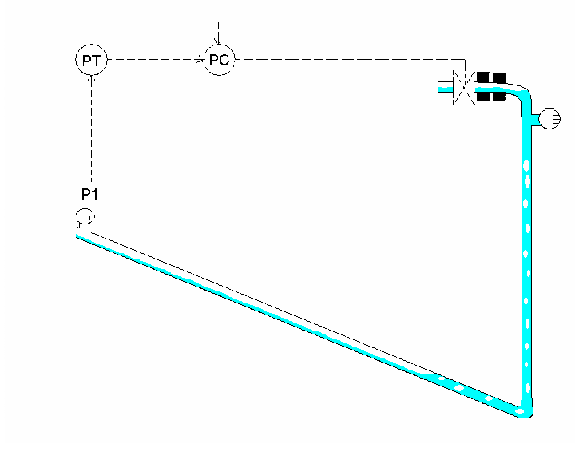

Fig. 12. Feedback control using PI controller with inlet pressure P_1 as measurement

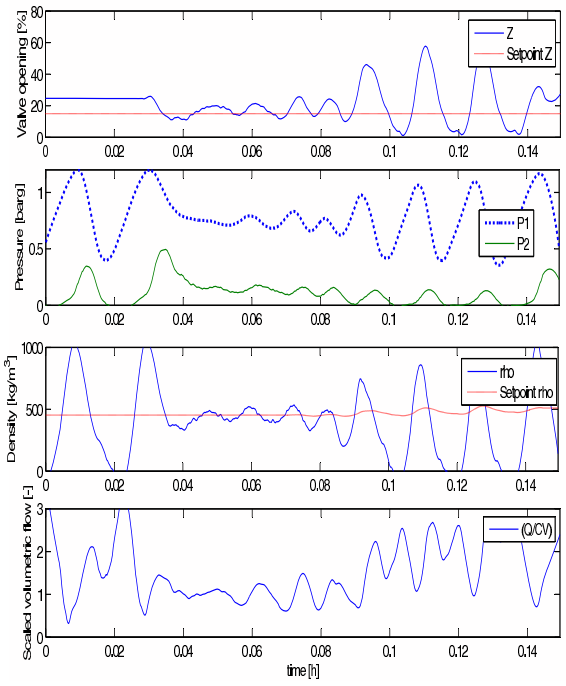

Fig. 14. Experimental results using a single measurement ρ in an attempt to stabilize the flow

Table 4. Mean values just before instability using different cascade controllers, based on data plotted in Figure 19

Outer loop	z			P_2		
Inner loop	P_1	ρ	F_Q/C_v	P_1	ρ	F_Q/C_v
$P_1[barg]$	0.71	0.68	0.68	0.72	0.72	0.67
$P_2[barg]$	0.146	0.123	0.119	0.132	0.142	0.079
$\rho[kg/m^3]$	425	433	403	424	433	417
$Q/C_v[-]$	1.18	0.98	1.18	1.28	1.0943	0.997
$z[\%]$	20.9	19.5	22.8	23.8	19.3	23.9
$F_w[m^3/h]$	7.24	7.55	7.6	7.54	7.60	7.55
$F_g[m^3/h]$	7.53	10.07	9.2	8.17	8.56	11.05
$Figure$	19(a)	19(b)	19(c)	19(d)	19(e)	19(f)

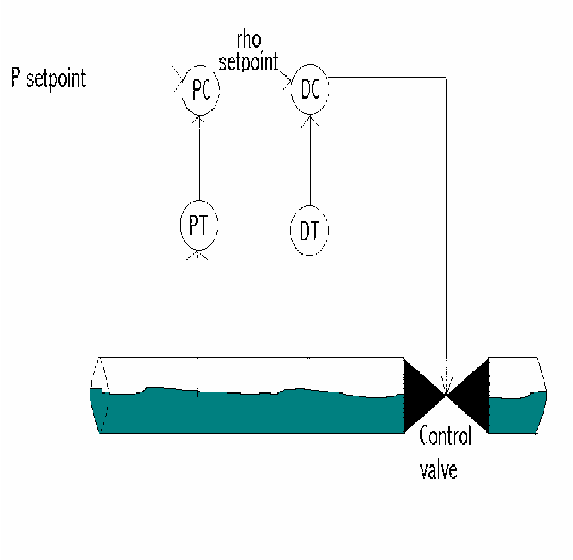

Fig. 15. Cascade control with measurements density ρ (inner loop) and pressure drop across topside valve P_2 (outer loop)

experimental results were far better than the model predicted when using the density as measurement.

During the experiments it was clear that the timing for when the controller is activated (where in the slug-cycle) is very important. When the controller was activated just after the inlet pressure had peaked, the controller managed to stabilize the flow quite easily. If the controller was activated at some other time, usually the controller didn't manage to stabilize the flow at all.

Also, the tuning of the controllers has a big influence on the results. Even better results might be achieved with other types of controllers or better tuning. This is also why it is not possible to make a clear recommendation of which combination of measurements is best. The study does however show that all the combinations stabilize the flow quite well.

6. CONCLUSION

This paper has presented results from a medium-scale riser rig where the aim was to control the flow using only topside measurements. The results show that it was possible to stabilize the flow using different combinations of topside measurements. Table 4 shows the different controller results compared to each other. The best results were achieved with the scaled volumetric flow rate F_Q/C_v as the inner measurements, although this result may be dependent on the tuning of the controllers. All of the controllers managed to stabilize the flow well, increasing the maximum valve opening from 12% without control to more than 20% with control.

When comparing the results with similar experiments performed on a small-scale riser rig build at our department, Sivertsen and Skogestad (2008), it seems like, despite the difference in size, the results using different control configurations are quite similar. This suggests that the small-scale riser rig might be suitable for testing different control strategies prior to more costly and time-consuming tests on larger rigs.

APPENDIX

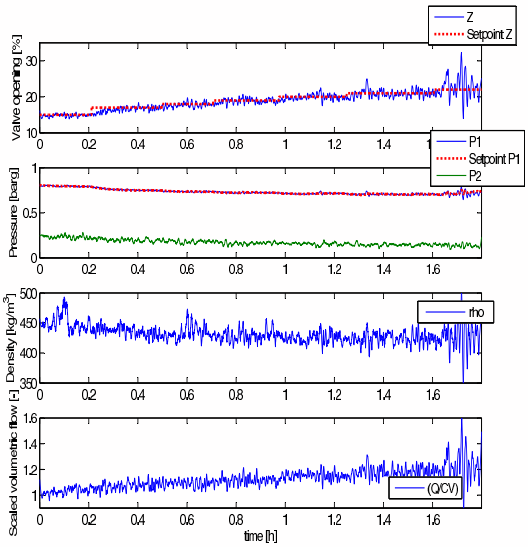

(a) z and P_1

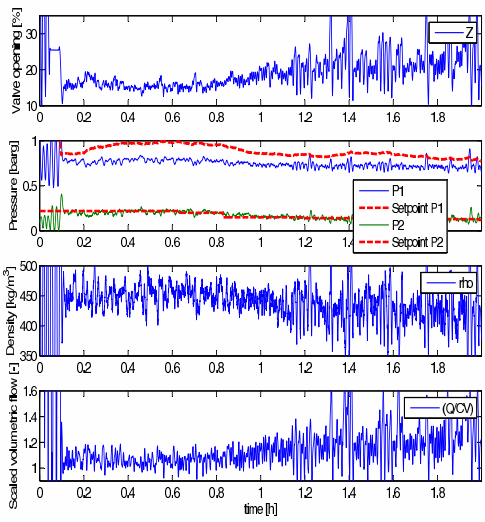

(b) P_2 and P_1

Fig. 16. Experimental results using P_1 in the outer loop and a) z and b) P_2 in the inner loop

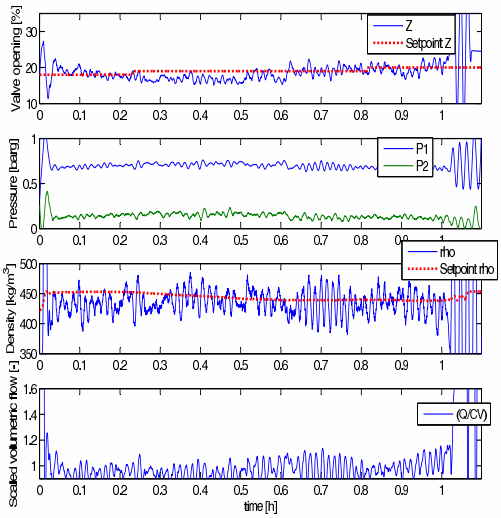

(a) z and ρ

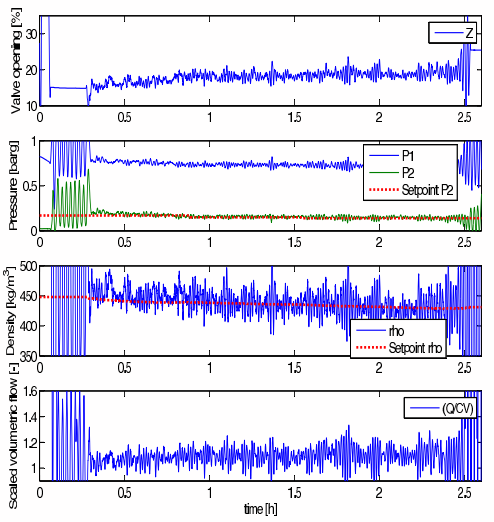

(b) P_2 and ρ

Fig. 17. Experimental results using ρ in the outer loop and a) z and b) P_2 in the inner loop

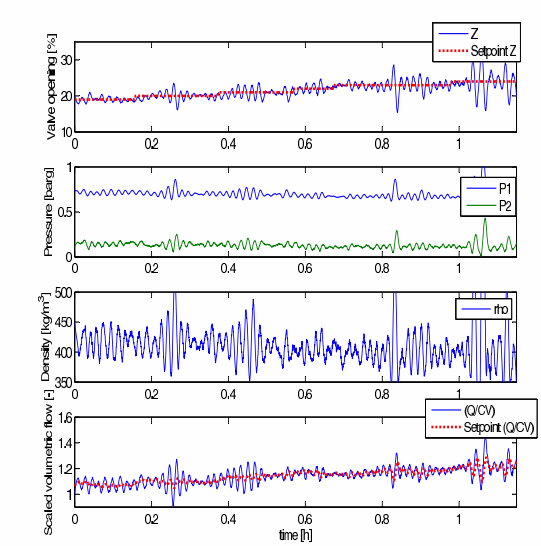

(a) z and F_Q

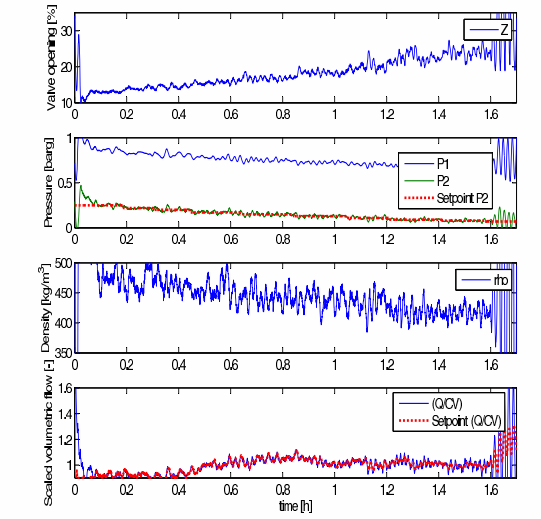

(b) P_2 and F_Q

Fig. 18. Experimental results using F_Q in the outer loop and a) z and b) P_2 in the inner loop

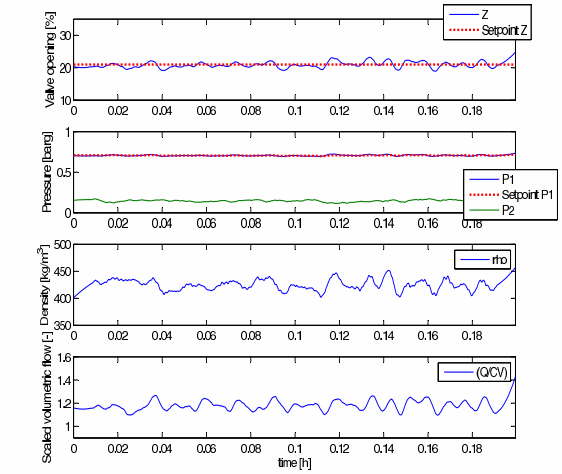

(a) P1andz22

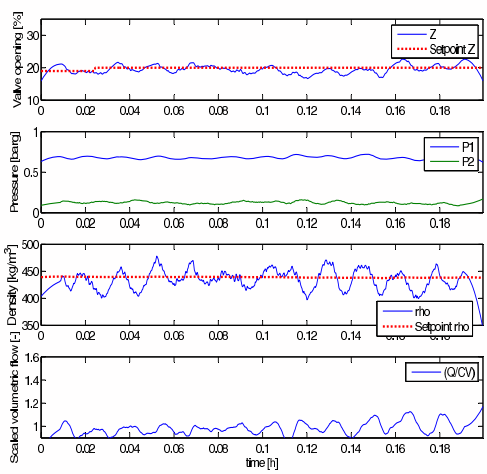

(b) Dandz20

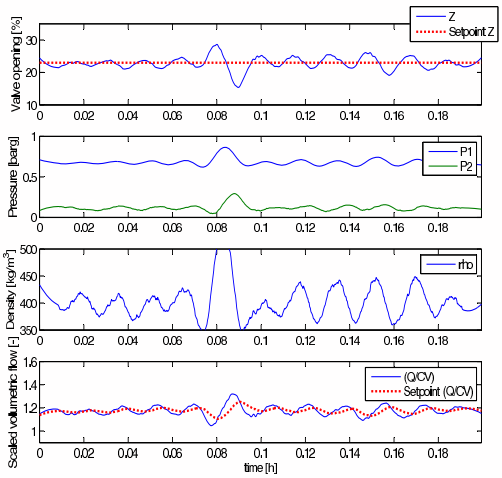

(c) Qandz23

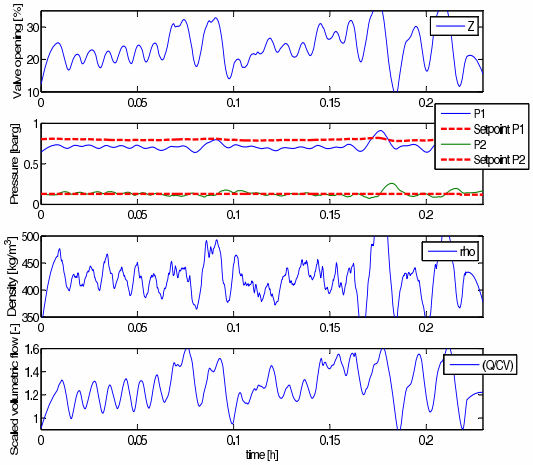

(d) P1andP213

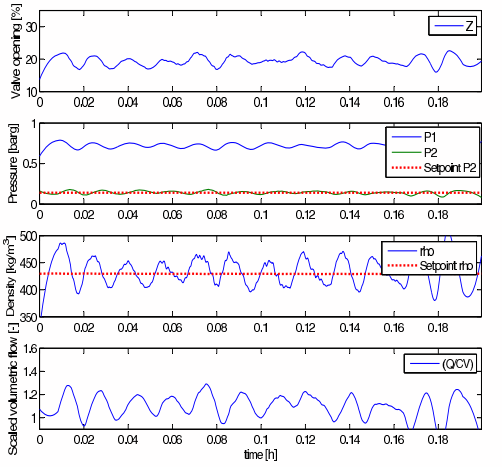

(e) DandP214

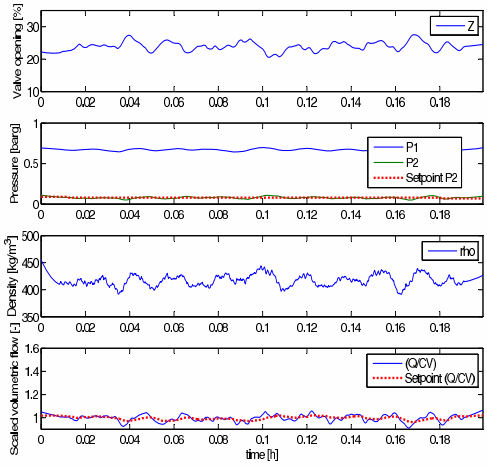

(f) QandP208

Fig. 19. Experimental results using six different combinations of measurements, last 12 min before instability

REFERENCES

H. Sivertsen and S. Skogestad. Experiments of riser slug flow using topside measurements: Part i. 2008.

S. Skogestad and I. Postlethwaite. *Multivariable feedback control*. John Wiley & sons, 1996.

E. Storkaas, S. Skogestad, and J.M. Godhavn. A low-dimentional model of severe slugging for controller design and analysis. In *Proceedings of multiphase '03, San Remo, Italy, 11-13 June 2003*, 2003.